THE JOURNAL OF PHYSICAL CHEMISTRY B

ARTICLE

pubs.acs.org/JPCB

Infrared Probing of 4-Azidoproline Conformations Modulated by Azido Configurations

Kyung-Koo Lee,[†] Kwang-Hee Park,[†] Cheonik Joo,[†] Hyeok-Jun Kwon,[†] Jonggu Jeon,[†] Hyeon-Il Jung,[†] Sungnam Park,[†,‡] Hogyu Han,[*,†] and Minhaeng Cho[*,†,‡]

[†]Department of Chemistry, Korea University, Seoul 136-701, Korea

[‡]Multidimensional Spectroscopy Laboratory, Korea Basic Science Institute, Seoul 136-713, Korea

Supporting Information

ABSTRACT: 4-Azidoproline (Azp) can tune the stability of the polyproline II (P_{II}) conformation in collagen. The azido group in the 4*R* and 4*S* configurations stabilizes and destabilizes the P_{II} conformation, respectively. To obtain insights into the dependence of the conformational stability on the azido configuration, we carried out Fourier transform (FT) IR experiments with four 4-azidoproline derivatives, Ac-(4*R*/*S*)-Azp-(NH/O)Me. We found that the amide I and azido IR spectra are different depending on the azido configuration and C-terminal structure. The origin of such spectral differences between 4*R* and 4*S* configurations and between C-terminal methylamide and ester ends was elucidated by quantum chemistry calculations in combination with ^{1}H NMR and time- and frequency-resolved IR pump−probe spectroscopy. We found that the azido configurations and C-terminal structures affect intramolecular interactions, which are responsible for the ensuing conformational and thereby IR spectral differences. Consequently, 4-azidoproline conformations modulated by azido configurations can be probed by IR spectroscopy. These findings suggest that 4-azidoproline can be both a structure-control and -probing element, which enables the infrared tracking of proline roles in protein structure, function, and dynamics.

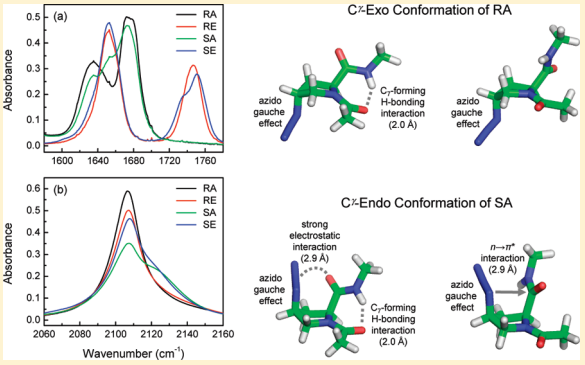

I. INTRODUCTION

Proline (Pro) residues play a unique and important role in protein structure, function, and dynamics.[1−11] In particular, the cis−trans isomerization of the peptidyl−prolyl bond is critically involved in the conformations and activities of peptides and proteins (Figures 1 and 2).[12,13] It has been suggested that the s-trans conformation is stabilized by $n \rightarrow \pi^*$ electronic delocalization, wherein an oxygen (O_{i-1}) lone pair (n) of a peptide bond overlaps with the carbonyl ($C'_i{=}O_i$) antibonding orbital (π^*) of the subsequent peptide bond (Figure 3, left).[14−16] This noncovalent interaction can be attenuated in the seven-membered cyclic γ-turn (C_7) structure, which is favorably formed in nonpolar or aprotic solvents by an intramolecular hydrogen-bonding interaction between two peptide bonds ($C'_{i-1}{=}O\cdots H{-}N_{i+1}$) (Figure 3, right).[17−23] Note that the C_7-forming H-bonding interaction contributes to the preference of the peptide bond for the s-trans conformation.

The side-chain modification of proline residues can influence the equilibrium populations of the s-trans and s-cis conformers.[24−39] Various substituents at C^β or C^γ have been found to be effective for modulating the s-trans/s-cis ratio via their stereoelectronic effects. In 4-azidoproline (Azp), for example, the s-trans/s-cis ratio is different depending on the azido configuration.[33] When an azido group is installed on the C^γ atom of proline in the 4*R* (4*S*) configuration, the s-trans/s-cis ratio becomes higher (lower) in aqueous solution: PE (Ac-Pro-OMe), 5.3:1; RE (Ac-(4*R*)-Azp-OMe), 6.1:1; SE (Ac-(4*S*)-Azp-OMe), 2.6:1 (see Figure 1).[15,33] It has been suggested that the stereoelectronic effect of the electronegative substituents, like the gauche effect, is responsible for the azido configuration dependence of the s-trans/s-cis ratio.[25,28,33] The ensuing azido gauche effect in the 4*R* (4*S*) configuration enforces the C^γ-exo (C^γ-endo) conformation of the Azp pyrrolidine ring, wherein the above $n \rightarrow \pi^*$ interaction can stabilize more (less) effectively the s-trans conformer of RE (SE) in comparison to PE (Figure 4). Note that the ability of the $n \rightarrow \pi^*$ interaction to stabilize the s-trans conformer is affected by the internal rotation of the azido group around the $N^\delta{-}C^\gamma$ bond (Figure 5). Upon such internal rotation, the influence of the unfavorable steric (repulsive) interaction between the azido and C-terminal carbonyl groups on the $n \rightarrow \pi^*$ interaction changes more greatly in the C^γ-endo compared to C^γ-exo conformation. Thus, the azido configuration dependence of the s-trans/s-cis ratio can be modulated somehow by such internal rotation, which has not been investigated yet.

Received: September 7, 2010
Revised: April 1, 2011
Published: April 18, 2012

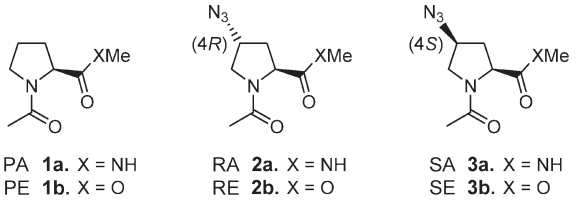

Figure 1. Structures of proline (PA and PE) and 4-azidoproline (RA, RE, SA, and SE) derivatives.

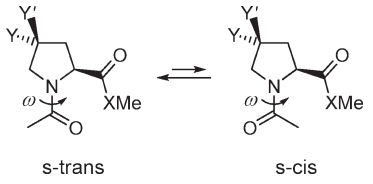

Figure 2. Cis−trans isomerization of the aminoacyl−prolyl peptide bond.

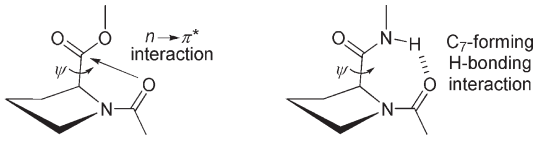

Figure 3. Intramolecular interactions determining stabilities of PA and PE. The s-trans conformer of PE is stabilized by the $n \rightarrow \pi^*$ interaction between the acetyl and ester groups (left). However, the s-trans conformer of PA is stabilized by the C_7-forming H-bonding interaction between the acetyl and amide groups particularly in nonpolar or aprotic solvents (right).

The C-terminal structure of proline residues can also affect the s-trans/s-cis ratio. For example, when the C-terminal structure of proline is changed from ester to amide, the s-trans/s-cis ratio becomes lower in aqueous solution: PE, 5.3:1; PA (Ac-Pro-NHMe), 2.6:1 (see Figure 1).[15,23] As mentioned above, the $n \rightarrow \pi^*$ and C_7-forming H-bonding interactions stabilize the s-trans conformers of PE and PA, respectively, and thus appear to be responsible for the C-terminal structure dependence of the s-trans/s-cis ratio (see Figure 3). This indicates that there could be differences in the involved intramolecular interactions and thereby the s-trans/s-cis ratio between RE and RA (Ac-(4*R*)-Azp-NHMe) and between SE and SA (Ac-(4*S*)-Azp-NHMe) (see Figure 1). That is, the azido configuration dependence of the s-trans/s-cis ratio can be modulated by C-terminal structures, which has not been clarified in detail yet.

Recently, we reported that β-azidoalanine can be a potentially useful IR probe of the local electrostatic environment in protein aggregates.[40,41] In addition, the β-azido group is an effective C_7-conformation-directing element, which may be useful for tuning the structures of other amino acids and polypeptides.[42] Accordingly, the β-azido group enables the control and IR-probing of protein structure, function, and dynamics.[43,44] 4-Azidoproline has also been used to tune the stability of the polyproline II (P_{II}) conformation in collagen, which mainly contains proline and hydroxyproline residues.[34] It was found that the azido group in the 4*R* and 4*S* configurations stabilizes and destabilizes the P_{II} conformation, respectively. This is largely due to

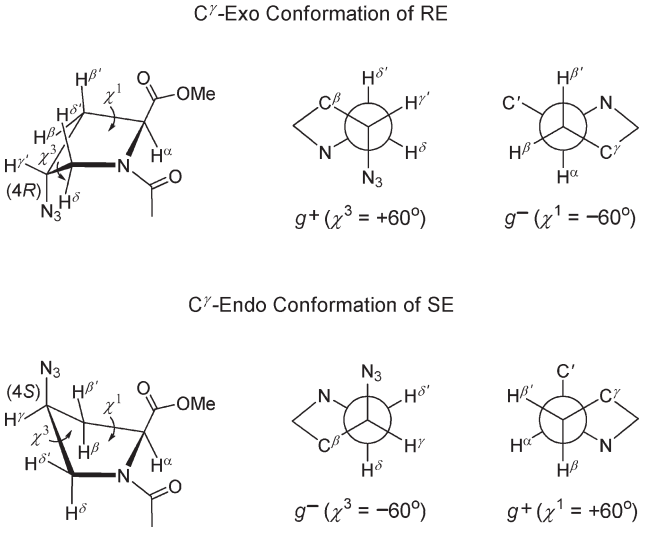

Figure 4. C^γ-exo and C^γ-endo conformations of the Azp pyrrolidine ring. Here, only the C^γ-exo and C^γ-endo conformations are depicted for the 4*R* and 4*S* configurations of the azido group in Azp, respectively. The azido gauche effects are involved in the stabilization of such conformations, where the azido group is in a *gauche* conformation relative to the *N*-acetyl group and thus in the pseudoaxial position. The Newman projections of two conformers viewed down the $C^\gamma-C^\delta$ bond axis clearly illustrate the gauche relationship between the pseudoaxial azido and *N*-acetyl groups, where the dihedral angle χ^3 ($N-C^\delta-C^\gamma-N^\delta$) is shown in their fully staggered conformations rather than geometry-optimized structures.[61] When the C^γ-endo (C^γ-exo) rather than C^γ-exo (C^γ-endo) conformation is depicted for the 4*R* (4*S*) configuration, the azido group is in an *anti* conformation relative to the *N*-acetyl group and thus in the pseudoequatorial position (Figure not shown). The Newman projections of two conformers viewed down the $C^\beta-C^\alpha$ bond axis are also depicted, where the dihedral angle χ^1 ($N-C^\alpha-C^\beta-C^\gamma$) is shown in their fully staggered conformations rather than geometry-optimized structures.[61]

the azido gauche effect that enforces the C^γ-exo (C^γ-endo) conformation for the 4*R* (4*S*) configuration. Note that, in such a conformation, the $n \rightarrow \pi^*$ interaction can stabilize more (less) effectively the s-trans conformer of RE (SE) in comparison to PE (see Figure 4). However, the potential of 4-azidoproline as a useful IR probe has not been addressed in detail yet.

Here, we report the study of 4-azidoproline to characterize its potential as an IR probe. We prepared its four derivatives, Ac-(4*R*/*S*)-Azp-(NH/O)Me, and carried out their comparative Fourier transform (FT) IR experiments (see Figure 1). Intriguingly, the amide I and azido IR spectra are found to be different depending on the azido configuration and C-terminal structure. To gain insights into the IR spectral dependence on the azido configuration and C-terminal structure, we performed quantum chemistry calculations in combination with ^{1}H NMR and time- and frequency-resolved IR pump−probe spectroscopic studies. We found that the azido configurations and C-terminal structures affect various intramolecular interactions, which interplay with each other to make the ensuing conformational and thereby IR spectral differences. These results indicate that 4-azidoproline conformations modulated by azido configurations can be probed by IR spectroscopy. Consequently, 4-azidoproline can be both a structure-control and -probing element, whereby the IR probing strategy can be further extended to the tracking of proline roles in protein structure, function, and dynamics.

dx.doi.org/10.1021/jp1085119 |*J. Phys. Chem. B* 2012, 116, 5097–5110

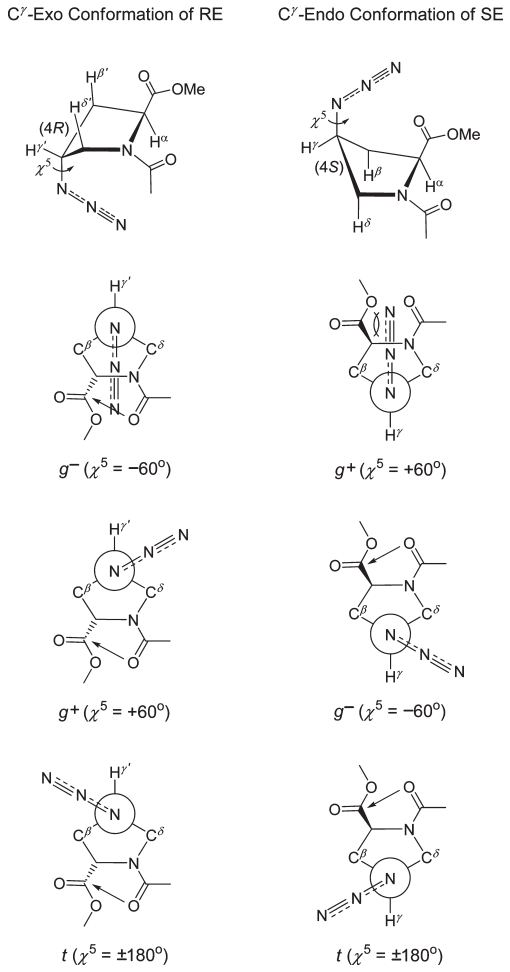

Figure 5. Internal rotation of the azido group in RE and SE. The Newman projections of three conformers viewed down the $N^{\delta}-C^{\gamma}$ bond axis are depicted, where the dihedral angle χ^5 ($C^{\delta}-C^{\gamma}-N^{\delta}-N^{\varepsilon}$) is shown in their fully staggered conformations rather than geometry-optimized structures. The $n \rightarrow \pi^*$ interaction between the *N*-acetyl carbonyl oxygen atom's nonbonding orbital (n) and the ester carbonyl group's antibonding orbital (π^*) is indicated by an arrow.

II. EXPERIMENTAL AND AB INITIO CALCULATION METHODS

A. Materials. Compounds **1**−**3** were synthesized and characterized (Scheme 1).

B. Sample Preparation. Spectroscopic grade chloroform ($CHCl_3$) was purchased from Sigma-Aldrich and used as received. Compounds **1**−**3** were directly dissolved in $CHCl_3$ to a concentration of ∼30 mM. At this concentration, there was no indication of sample aggregation. For FTIR and IR pump−probe experiments, all samples were placed in a cell with two 2 mm thick CaF_2 windows and a 100 μm thick Teflon spacer. FTIR spectra were measured before and after the IR pump−probe experiments to check the undesired sample degradation during the experiments. We found that there was no significant change in the FTIR spectra.

C. FTIR Spectroscopy. To obtain the conformational distributions of four 4-azidoproline derivatives in $CHCl_3$, FTIR spectra were measured on a JASCO FT/IR-4100 spectrometer equipped with a HgCdTe detector. FTIR spectra were measured with a resolution of 1 cm^{-1} at 21 °C. The background spectrum was obtained with $CHCl_3$ in the same sample cell and was subtracted. For quantitative analyses, the C═O stretch bands (1600−1700 cm^{-1}) of (methyl)amides, C═O stretch bands (∼1740 cm^{-1}) of esters, and azido stretch bands (∼2100 cm^{-1}) were fitted to multiple Gaussian, Lorentzian, or Voigt functions.

D. NMR Spectroscopy. To quantitatively determine the s-trans/s-cis ratios for four 4-azidoproline derivatives in $CDCl_3$, ^{1}H NMR spectra were measured on a Varian VnmrS600 NMR

Scheme 1. Syntheses of Compounds 1−3[a]

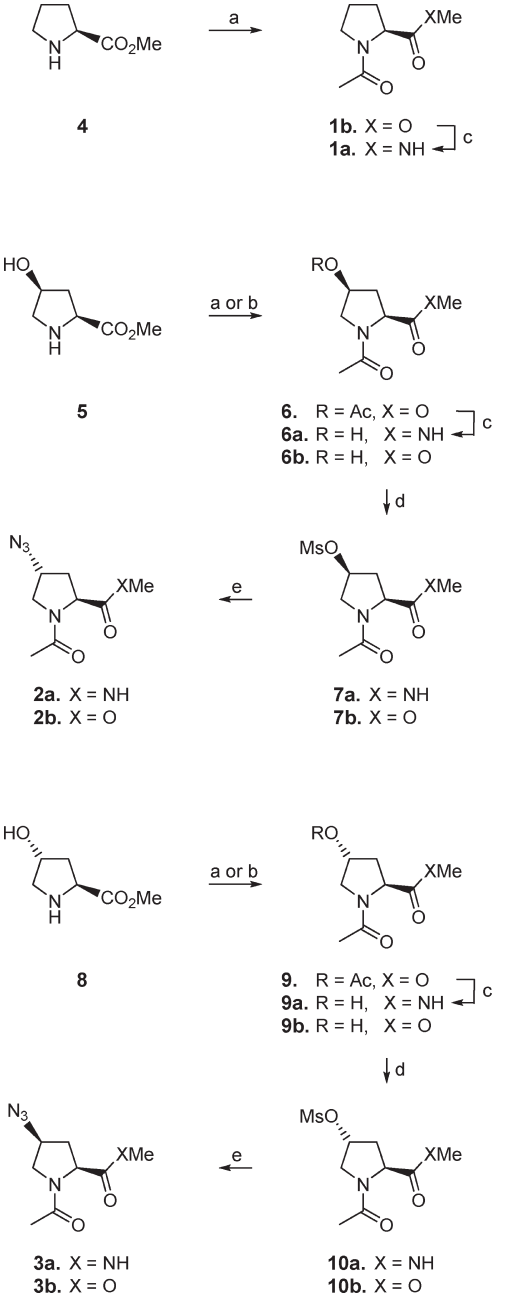

[a] Reagents and conditions: (a) Ac_2O, Et_3N, DMAP, CH_2Cl_2, rt (**1b**, 85%; **6**, 86%; **9**, 97%); (b) AcOH, Et_3N, DMAP, EDCI, DMF, rt (**6b**, 50%; **9b**, 42%); (c) 40% $MeNH_2$, MeOH, rt (**1a**, 78%; **6a**, 96%; **9a**, 84%); (d) MsCl, Et_3N, CH_2Cl_2, −10 °C and then rt; (e) NaN_3, DMF, 55 or 60 °C (**2a**, 67%; **2b**, 94%; **3a**, 54%; **3b**, 89%).

dx.doi.org/10.1021/jp1085119 |*J. Phys. Chem. B* 2012, 116, 5097–5110

Table 1. s-trans:s-cis Conformer Ratios for Proline and 4-Azidoproline Derivatives in $CDCl_3$ at 25 °C[a]

compounds	s-trans:s-cis
PA	6.9:1
PE	4.0:1[b]
RA	12.2:1
RE	3.9:1[c]
SA	2.6:1
SE	1.9:1[c]

[a] s-trans/s-cis ratios are determined by ^{1}H NMR spectroscopy. [b] See Table 1 in ref 15. [c] See Table 1 in ref 33. 600 MHz ^{1}H NMR spectral analyses of RA and SA are shown in Table S1 of the Supporting Information.

spectrometer. More specifically, the chemical shift of the methyl protons in the *N*-acetyl group differs between the s-trans and s-cis conformers and the corresponding integrated areas are used to determine the s-trans/s-cis ratio. The s-trans/s-cis ratios for all the compounds studied here are summarized in Table 1.

E. Time-Resolved IR Pump−Probe Spectroscopy. To measure the population relaxation dynamics of azido stretch modes, we carried out time-resolved IR pump−probe experiments using femtosecond IR pulses. The mid-IR pulse from our laser system was centered at ∼2070 cm^{-1} with a bandwidth of ∼250 cm^{-1}, which was broad enough to cover the entire azido IR band.[45] The mid-IR pulse was properly precompensated by CaF_2 plates for the optical components in the setup, producing a transform-limit pulse at the sample position.[45,46] For IR pump−probe experiments, the mid-IR pulse was split into the pump and probe beams, which were focused onto the sample by a parabolic mirror (f.l. = 10 cm). The probe beam was collimated by another parabolic mirror (f.l. = 10 cm) after the sample and was dispersed in a monochromator onto a 64-element MCT array detector.[47] In IR pump−probe experiments, the pump pulse excites a molecular system to the first vibrational excited state (v = 1) and subsequently the relaxation of the molecular system is monitored by the probe beam as a function of time-delay (t). The IR pump−probe signal decays as a result of the vibrational population and orientational relaxations.[47,48] To selectively measure the population relaxation decay, $P(t)$, the IR pump−probe signal was collected in a magic angle geometry, where the polarization of the probe beam was set to be 54.7° with respect to that of the pump beam. In this particular polarization geometry, the orientational relaxation is averaged out and does not contribute to the IR pump−probe signal.

F. Quantum Chemistry Calculations. To investigate the conformational propensities and intramolecular interactions in four 4-azidoproline derivatives, we carried out quantum chemistry calculations with density functional theory (DFT) at the B3LYP/6-311++G** level in the Gaussian 03 suite.[49] To take into account the solvation effect, we used the integral equation formalism for the polarizable continuum model (IEFPCM).[50,51] A simple united atom topological model was used, and the dielectric constant was assumed to be 4.9. Because the 4-azidoproline derivatives can have various conformations depending on the backbone and side-chain dihedral angles, we considered only 12 input structures with the three dihedral angles ω, χ^1, and χ^5 defined initially (see Figures 2, 4, and 5). They are different depending on the conformations of the *N*-acetyl group (s-trans and s-cis), the pyrrolidine ring (C^γ-endo and C^γ-exo), and the azido group (*trans* (t), *gauche*+ (g^+), and *gauche*− (g^-)), which are defined by the three dihedral angles ω, χ^1, and χ^5, respectively. The geometry optimization was carried out starting from these initial input geometries without any further constraints. In addition, the quantum chemistry calculation was performed for both the s-trans and s-cis conformers of PA as reference molecules for comparisons with 4-azidoproline derivatives.

It should be noted that the DFT-IEFPCM calculations are much better than just the DFT calculations for isolated molecules. We carried out the DFT calculations too, but the relative energies of 4-azidoproline derivatives, which are related to their percent populations, were not in good agreement with the experimental (NMR) results on the s-trans/s-cis ratios. We have not tried the explicit solute−solvent cluster approach here, because it was not clear how many solvent (chloroform) molecules were to be included to get reasonable results. Nevertheless, all the molecular structures shown here were obtained from the DFT-IEFPCM calculations at the B3LYP/6-311++G** level.

III. RESULTS AND DISCUSSION

A. NMR Spectra and Quantum Chemistry Calculations: Conformational Propensities and Intramolecular Interactions. To study the stereoelectronic effect of the azido group on the conformation of 4-azidoproline (Azp), we carried out NMR experiments and quantum chemistry calculations for its four derivatives, Ac-(4*R*/*S*)-Azp-(NH/O)Me (see Figure 1). For comparative analysis of their conformational propensities and intramolecular interactions, we first focused on two proline (Pro) derivatives Ac-Pro-(NH/O)Me as reference compounds (see Figure 1).[52−54] It is known that the backbone conformation of Ac-Pro-NH_2 is highly sensitive to local solvent environments: P_{II} in polar protic solvents such as water and alcohols but C_7 in less-polar aprotic solvents such as chloroform.

Ac-Pro-XMe. ^{1}H NMR spectra of PA (PE) (PA, X = NH; PE, X = O) in $CDCl_3$ showed two nine (eight)-spin systems, which correspond to the s-trans and s-cis conformers. In both PA and PE, the s-trans conformer was the major form. However, the s-trans/s-cis ratio for PA was higher than that for PE (6.9 vs 4.0, see Table 1). Thus, the s-trans/s-cis ratio is different depending on the C-terminal structure of Pro. The s-trans conformer of PA is stabilized by the intramolecular C_7-forming H-bonding interaction between two peptide bonds (see Figure 3, right). However, that of PE is stabilized by the intramolecular $n \rightarrow \pi^*$ interaction between the *N*-acetyl carbonyl oxygen atom's nonbonding orbital (n) and the ester carbonyl group's antibonding orbital (π^*) (see Figure 3, left). Consequently, it appears that the C_7-forming H-bonding interaction is more effective in stabilizing the s-trans conformer than such $n \rightarrow \pi^*$ interaction, thereby affording the higher s-trans/s-cis ratio for PA compared to PE.

Ac-(4R)-Azp-XMe. ^{1}H NMR spectra of RA (RE) (RA, X = NH; RE, X = O) in $CDCl_3$ showed two nine (eight)-spin systems, which correspond to the s-trans and s-cis conformers. In both RA and RE, the s-trans conformer was the major form. However, the s-trans/s-cis ratio for RA was significantly higher than that for RE (12.2 vs 3.9, see Table 1). Thus, the s-trans/s-cis ratio is different depending on the C-terminal structure of Azp. The s-trans/s-cis ratio for RA (RE) was even much higher than (almost equal to) that for PA (PE) (12.2 (3.9) vs 6.9 (4.0)). Thus, the azido substituent at C^γ appears to be responsible for the difference in such conformer ratio. The pyrrolidine ring of Azp can adopt two main structures, a C^γ-endo or C^γ-exo conformation (see Figure 4).

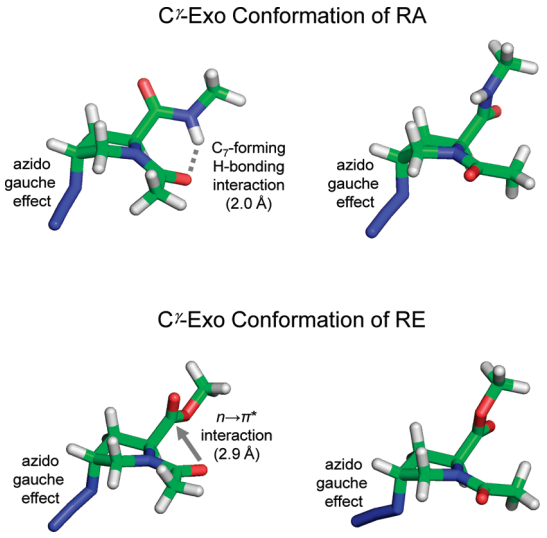

Figure 6. Geometry-optimized structures of the C$^\gamma$-exo puckers of the s-trans (left) and s-cis (right) conformers in RA and RE. Note that when RA and RE adopt the C$^\gamma$-exo conformation, the azido substituent occupies the pseudoaxial position. The intramolecular interactions stabilizing such structures are indicated. See the detailed discussion in section III.A. For comparison, the C$^\gamma$-endo structures of the s-trans and s-cis conformers in RA and RE are depicted and the intramolecular interactions stabilizing those structures are indicated in Figure S1 of the Supporting Information. Color coding: white, hydrogen; green, carbon; blue, nitrogen; red, oxygen.

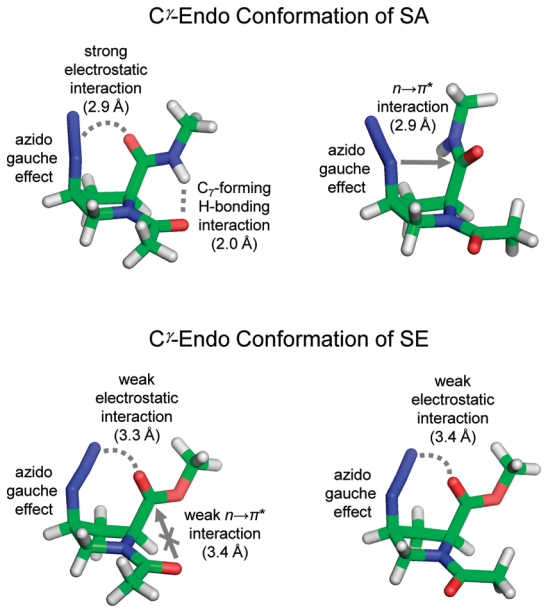

Figure 7. Geometry-optimized structures of the C$^\gamma$-endo puckers of the s-trans (left) and s-cis (right) conformers in SA and SE. Note that when SA and SE adopt the C$^\gamma$-endo conformation, the azido substituent occupies the pseudoaxial position. The intramolecular interactions stabilizing such structures are indicated. See the detailed discussion in section III.A. For comparison, the C$^\gamma$-exo structures of the s-trans and s-cis conformers in SA and SE are depicted and the intramolecular interactions stabilizing those structures are indicated in Figure S2 of the Supporting Information. Color coding: white, hydrogen; green, carbon; blue, nitrogen; red, oxygen.

From the ^{1}H NMR coupling constants, we found that both the s-trans and s-cis conformers of RA adopt the C$^\gamma$-exo conformation, where the azido substituent occupies the pseudoaxial position (Table S1 of the Supporting Information). Likewise, it is found that both the s-trans and s-cis conformers of RE adopt the C$^\gamma$-exo conformation (see Table S1 of the Supporting Information).

To elucidate the confomational propensities of RA and RE, we carried out quantum chemistry calculations with DFT-IEFPCM at the B3LYP/6-311++G** level in the Gaussian 03 suite (see details in section II.F). The relative calculated electronic energies of 12 conformers for each of RA and RE are summarized in Table S2 of the Supporting Information. Here, the energy-minimum structures of both RA and RE adopt the s-trans and C$^\gamma$-exo conformations. In Figure 6, the geometry-optimized structures of the C$^\gamma$-exo puckers of the s-trans and s-cis conformers in RA and RE are depicted and the intramolecular interactions stabilizing those structures are indicated. Note that both the s-trans and s-cis conformers of RA and RE adopt the C$^\gamma$-exo conformation. To understand the structural preferences of RA and RE, the intramolecular interactions need to be examined. First of all, the s-trans conformer of RA is stabilized by the intramolecular C$_7$-forming H-bonding interaction between two peptide bonds. However, that of RE is stabilized by the intramolecular $n \rightarrow \pi^*$ interaction between the *N*-acetyl carbonyl oxygen atom's nonbonding orbital (n) and the ester carbonyl group's antibonding orbital (π^*). Note that these two interactions are the original elements stabilizing the s-trans conformers of PA and PE as described above (see Figure 3). Additionally, the azido gauche effects are involved in the stabilization of all four structures, where the azido group is in a *gauche* rather than *anti* conformation relative to the *N*-acetyl group. Accordingly, the four structures in Figure 6 have a different number and type of intramolecular interactions, which determine their relative stabilization energies. For comparison, the C$^\gamma$-endo structures of the s-trans and s-cis conformers in RA and RE are depicted and the intramolecular interactions stabilizing those structures are indicated in Figure S1 of the Supporting Information.

Note that, from the ^{1}H NMR spectra, RA (RE) is found to have the s-trans/s-cis ratio of 12.2 (3.9), which is much higher than (almost equal to) 6.9 (4.0) for PA (PE) (see Table 1). By closely comparing all the intramolecular interactions in Figures 3 and 6, we may conclude that the much higher (almost equal) s-trans/s-cis ratio for RA (RE) compared to PA (PE) is attributed to the azido gauche effect. This is because such interaction is present only in RA and RE but not in PA and PE. Interestingly, however, the azido gauche effect is present in both the s-trans and s-cis conformers of RA and RE, determining their C$^\gamma$-exo conformation.[33] If this interaction alone determines the stability of the s-trans and s-cis conformers of RA and RE, the s-trans/s-cis ratio for RA would be the same as that for RE. Thus, we can deduce that the azido gauche effect should interplay with other interactions to determine their relative stabilities. Clearly, there are additional interactions such as the C$_7$-forming H-bonding interaction and the $n \rightarrow \pi^*$ interaction in the s-trans conformers of RA and RE, respectively. Consequently, it appears that the C$_7$-forming H-bonding interaction in the s-trans conformer of RA becomes stronger upon its C$^\gamma$-exo adoption, thereby affording the much higher s-trans/s-cis ratio for RA compared to PA (12.2 vs 6.9). In contrast, the $n \rightarrow \pi^*$ interaction in the s-trans conformer of RE is rarely affected by its C$^\gamma$-exo adoption, thereby affording nearly the same s-trans/s-cis ratio for both RE and PE (3.9 vs 4.0).

dx.doi.org/10.1021/jp1085119 |*J. Phys. Chem. B* 2012, 116, 5097–5110

Ac-(4S)-Azp-XMe. ^{1}H NMR spectra of SA (SE) (SA, X = NH; SE, X = O) in $CDCl_3$ showed two nine (eight)-spin systems, which correspond to the s-trans and s-cis conformers. In both SA and SE, the s-trans conformer was the major form, although the s-trans/s-cis ratio for SA was slightly higher than that for SE (2.6 vs 1.9, see Table 1). Thus, the s-trans/s-cis ratio is rarely dependent on the C-terminal structure of Azp. The s-trans/s-cis ratio for SA (SE) was much lower than that for PA (PE) (2.6 (1.9) vs 6.9 (4.0)) and RA (RE)(2.6 (1.9) vs 12.2 (3.9)). Thus, both the azido substituent at C^γ and its configuration appear to be responsible for the difference in such conformer ratio. The pyrrolidine ring of Azp can adopt two main structures, a C^γ-endo or C^γ-exo conformation (see Figure 4). From the ^{1}H NMR coupling constants, we found that both the s-trans and s-cis conformers of SA adopt the C^γ-endo conformation, where the azido substituent occupies the pseudoaxial position (see Table S1 of the Supporting Information). Likewise, it is found that both the s-trans and s-cis conformers of SE adopt the C^γ-endo conformation (see Table S1 of the Supporting Information).

To elucidate the confomational propensities of SA and SE, we carried out quantum chemistry calculations with DFT-IEFPCM at the B3LYP/6-311++G** level in the Gaussian 03 suite (see details in section II.F). The relative calculated electronic energies of 12 conformers for each of SA and SE are summarized in Table S2 of the Supporting Information. Here, the energy-minimum structures of both SA and SE adopt the s-trans and C^γ-endo conformations. In Figure 7, the geometry-optimized structures of the C^γ-endo puckers of the s-trans and s-cis conformers in SA and SE are depicted and the intramolecular interactions stabilizing those structures are indicated. Note that both the s-trans and s-cis conformers of SA and SE adopt the C^γ-endo conformation. To understand the structural preferences of SA and SE, the intramolecular interactions need to be examined. First of all, the s-trans conformer of SA is stabilized by the intramolecular C_7-forming H-bonding interaction between two peptide bonds. However, that of SE is no longer stabilized by the intramolecular $n \rightarrow \pi^*$ interaction between the *N*-acetyl carbonyl oxygen atom's nonbonding orbital (n) and the ester carbonyl group's antibonding orbital (π^*). Note that these two interactions are the dominant factors stabilizing the s-trans conformers of PA (RA) and PE (RE) as described above (see Figures 3 and 6). Additionally, the azido gauche effects are involved in the stabilization of all four structures, where the azido group is in a *gauche* rather than *anti* conformation relative to the *N*-acetyl group. Finally, the azido group makes intramolecular interactions with the C-terminal carbonyl oxygen and carbon atoms: (1) strong electrostatic interaction between the azido central N^ε atom and the methylamide carbonyl O atom in the s-trans conformer of SA, (2) $n \rightarrow \pi^*$ interaction between the azido inner N^δ atom covalently bonded directly to C^γ and the methylamide carbonyl C atom in the s-cis conformer of SA, and (3) weak electrostatic interaction between the azido terminal N^ζ atom and the ester carbonyl O atom in both the s-trans and s-cis conformers of SE. Accordingly, the four structures in Figure 7 have a different number and type of intramolecular interactions, which determine their relative stabilization energies. For comparison, the C^γ-exo structures of the s-trans and s-cis conformers in SA and SE are depicted and the intramolecular interactions stabilizing those structures are indicated in Figure S2 of the Supporting Information.

Note that, from the ^{1}H NMR spectra, SA (SE) is found to have the s-trans/s-cis ratio of 2.6 (1.9), which is much lower than 6.9 (4.0) for PA (PE) and 12.2 (3.9) for RA (RE) (see Table 1). By closely comparing all the intramolecular interactions in Figures 3 and 7, we can conclude that the much lower s-trans/s-cis ratio for SA (SE) compared to PA (PE) and RA (RE) is attributed to the interplay between the interactions including the azido gauche effect. Furthermore, we can deduce that the azido gauche effect is the dominant interaction determining their relative stabilities. This is because, regardless of the other interactions, both the s-trans and s-cis conformers of SA and SE adopt the C^γ-endo conformation, which is suggested to be primarily determined by the azido gauche effect.[33] As discussed in the s-trans conformers of PA and RA, the C_7-forming H-bonding interaction stabilizes the s-trans conformer of SA. In addition, there is a strong electrostatic interaction between the azido central N^ε atom and the methylamide carbonyl O atom in the s-trans conformer of SA. In this case, the partial charge of the azido central N^ε atom is positive.[41] This additional interaction is facilitated by its C^γ-endo adoption whereupon the azido group occupies the pseudoaxial position close enough to make a strong electrostatic interaction with the negatively charged methylamide carbonyl O atom. Note that the distance between the azido central N^ε atom and the methylamide carbonyl O atom is about 2.9 Å. Thus, we can expect that these two interactions force the s-trans/s-cis ratio for SA to be higher than that for PA and RA. However, SA is found to have a lower s-trans/s-cis ratio compared to PA and RA. This seemingly contradictory situation can be resolved if we notice the $n \rightarrow \pi^*$ interaction between the azido inner N^δ atom and the methylamide carbonyl C atom in the s-cis conformer of SA. In this case, the electron donation of the azido inner N^δ atom's nonbonding orbital (n) into the methylamide carbonyl group's antibonding orbital (π^*) takes place. This interaction is facilitated by its C^γ-endo adoption whereupon the azido group occupies the pseudoaxial position close enough to make an $n \rightarrow \pi^*$ interaction with the methylamide carbonyl C atom. Note that the distance between the azido inner N^δ atom and the methylamide carbonyl C atom is about 2.9 Å and the angle between the direction of the $n \rightarrow \pi^*$ interaction and the amide plane of the methylamide group is close to 90°. Consequently, such interaction seems to make the s-cis conformer of SA stable enough to afford the much lower s-trans/s-cis ratio for SA compared to PA (RA) (2.6 vs 6.9 (12.2)). As discussed in the s-trans conformers of PE and RE, the $n \rightarrow \pi^*$ interaction between the *N*-acetyl carbonyl oxygen atom's nonbonding orbital (n) and the ester carbonyl group's antibonding orbital (π^*) stabilizes the s-trans conformers of the esters. Thus, we can deduce that the absence of such $n \rightarrow \pi^*$ interaction leads to a decrease in the s-trans/s-cis ratio for the esters. In the s-trans conformer of SE, its C^γ-endo adoption does not allow such $n \rightarrow \pi^*$ interaction.[33] Consequently, a lack of such $n \rightarrow \pi^*$ interaction seems to make the s-trans conformer of SE unstable enough to afford the much lower s-trans/s-cis ratio for SE compared to PE (RE) (1.9 vs 4.0 (3.9)).

In short, the lower s-trans/s-cis ratio for SA (SE) compared to PA (PE) and RA (RE) is due to the stabilization (destabilization) of the s-cis (s-trans) conformer of SA (SE) relative to PA (PE) and RA (RE). The s-cis conformer of SA is stabilized by the $n \rightarrow \pi^*$ interaction between the azido inner N^δ atom's nonbonding orbital (n) and the methylamide carbonyl group's antibonding orbital (π^*). On the other hand, the s-trans conformer of SE is destabilized by a lack of the $n \rightarrow \pi^*$ interaction between the *N*-acetyl carbonyl oxygen atom's nonbonding orbital (n) and the ester carbonyl group's antibonding orbital (π^*). Undoubtedly, these $n \rightarrow \pi^*$ interactions are made and broken effectively upon their C^γ-endo adoption, which is primarily determined by the azido gauche effect.

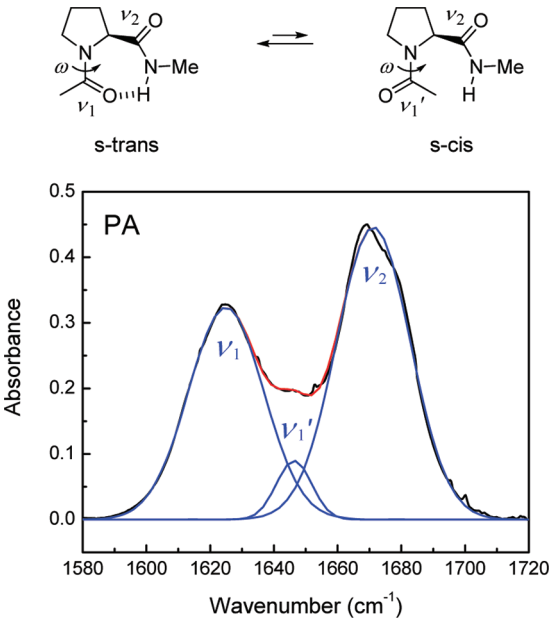

Figure 8. Amide I IR spectrum of PA in $CHCl_3$ and its factor analysis. See experimental details in sections II.B and II.C. The experimentally measured amide I IR spectrum (black) of PA can be fitted to the sum (red) of three Gaussian functions (blue) at the center frequencies of 1625 (ν_1), 1646 (ν_1'), and 1671 (ν_2) cm^{-1}. The two low (one high)-frequency bands ν_1 and ν_1' (ν_2) can be easily assigned to the amide I modes localized on the acetyl (methylamide)-end peptide groups of the respective (both the) s-trans and s-cis conformers in PA.[53,54] See the detailed discussion in section III.B. For quantitative fitting information, see Table S3 of the Supporting Information.

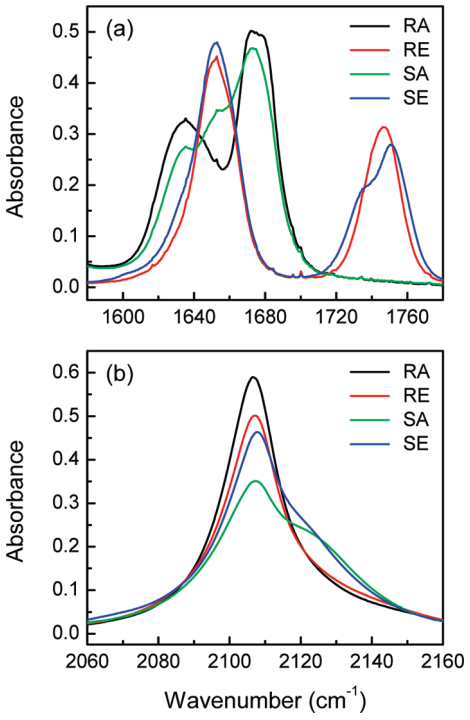

Figure 9. FTIR spectra of RA, RE, SA, and SE in $CHCl_3$. (a) Amide I bands of RA, RE, SA, and SE and the C═O stretch bands of RE and SE. (b) Azido stretch bands of RA, RE, SA, and SE. See experimental details in sections II.B and II.C. Factor analyses of IR spectra in (a) and (b) for SA and SE were carried out using Gaussian (or Voigt) and Lorentzian functions (Figure 10 and Figure S4 of the Supporting Information). See the detailed discussion in section III.B. For quantitative fitting information, see Table S3 of the Supporting Information.

Consequently, the azido gauche effect turns out to be a key factor modulating the stability of Azp conformers and thereby their ratios. Definitely, the relative conformational stabilities affected by the azido gauche effect are different depending on the azido configuration. In the next subsection, we will show that the Azp conformations modulated by the azido configurations subtly but distinctively via stereoelectronic effects can be probed by IR spectroscopy.

B. FTIR Spectra. To investigate the Azp conformations modulated by azido configurations, we carried out Fourier transform (FT) IR experiments with four Azp derivatives. For comparative analysis, we first focused on the Pro derivative PA as a reference compound.

Ac-Pro-(NH/O)Me. The amide I IR spectrum of PA in $CHCl_3$ is shown in Figure 8. At first sight, it appears to be a doublet with two peaks at 1625 and 1671 cm^{-1}. The low- and high-frequency bands can be easily assigned to the amide I vibrations relatively localized on the acetyl-end and methylamide-end peptide groups, respectively. Note that the acetyl-end peptide group of PA is the tertiary amide group, whereas its methylamide-end peptide group is the normal secondary amide group. Here, it should be mentioned that the amide I *local* modes of the two peptide groups are in fact coupled to each other. However, the coupling constant, which is typically in the range of a few wavenumbers,[52] is much smaller than the frequency difference (~46 cm^{-1}) between the two amide I local modes. Therefore, the amide I *normal* modes are fairly localized. It is also interesting to note that the low-frequency peak intensity appears to be slightly weaker than the high-frequency peak intensity. From this, one might suggest that the oscillator strength of the low-frequency amide I mode is smaller than that of the high-frequency component. Since the two amide I mode frequencies in PA are separated from each other, one could use the two-dimensional (2D) IR spectroscopic technique to resolve the cross-peak in the experimentally measured 2DIR spectrum. For PE, the amide I vibration at the acetyl end exhibits a singlet at 1641 cm^{-1} and the C═O stretching vibration at the ester end exhibits a singlet at 1743 cm^{-1} (data not shown).

To quantitatively estimate the relative oscillator strengths of the underlying components in the amide I IR spectrum of PA, we carried out its factor analysis using three Gaussian functions; note that the fitting quality with two Gaussian functions is comparatively poor. The three components are shown in Figure 8. In addition to the two underlying bands at 1625 (ν_1) and 1671 (ν_2) cm^{-1} discussed above, there is one weak band at 1646 (ν_1') cm^{-1}. Among the three, the two low-frequency ν_1- and ν_1'-bands can be safely assigned to the amide I modes localized on the acetyl-end peptide groups of the s-trans and s-cis conformers in PA, respectively.[53,54] On the other hand, the one high-frequency ν_2-band can be assigned to the amide I modes on the methylamide-end peptide groups of the s-trans and s-cis conformers in PA. Note that the s-trans conformer is spectrally distinguishable (indistinguishable) from the s-cis conformer in the amide I vibration at the acetyl (methylamide) end. The C_7-forming H-bonding interaction between the *N*-acetyl carbonyl O atom and the methylamide H atom in the s-trans conformer of PA is responsible for the red-shift (~21 cm^{-1} from ν_1' to ν_1) of its amide I vibration at the acetyl end.[54] The relative areas of the three amide I bands (ν_1, ν_1',

dx.doi.org/10.1021/jp1085119 |J. Phys. Chem. B 2012, 116, 5097–5110

and ν_2) in PA are found to be 7.71:1:10.48. The areas of individual peaks are directly proportional to the absorbance ($A = \varepsilon bC$).

From the NMR study, the s-trans/s-cis ratio for PA in $CDCl_3$ was found to be 6.9:1. Thus, the relative populations of the three amide I oscillators (ν_1, ν_1', and ν_2) in PA are 6.9:1:7.9. From the above IR study, the relative areas of the three amide I bands in PA are found to be 7.71:1:10.48. By combining these two results with Beer's law, the relative extinction coefficients of the three amide I modes (ν_1, ν_1', and ν_2) in PA can be determined to be 1.12:1:1.33. We will use these relative oscillator strengths to subsequently analyze the amide I IR spectrum of SA.

Before we close this subsection, it should be noted that the amide A IR spectrum of PA provides additional evidence on the relative populations of its s-trans and s-cis conformers. The amide A IR spectrum of PA in $CHCl_3$ appears to be a doublet with two peaks at 3327 and 3450 cm^{-1}(Figure S3 of the Supporting Information). The low-frequency band arises from the N−H stretch of the s-trans conformer having the C_7-forming H-bonding interaction, whereas the high-frequency band arises from the N−H stretch of the s-cis conformer having no such H-bonding interaction.[55] Note that both the C═O stretching vibrations (ν_1 and ν_1' in Figure 8) at the acetyl end and the N−H stretching vibrations (two bands at 3327 and 3450 cm^{-1} in Figure S3 of the Supporting Information) at the methylamide end are directly influenced by the C_7-forming H-bonding interaction.

Ac-(4R)-Azp-(NH/O)Me. In Figure 9, the amide I and azido IR spectra of RA and RE in $CHCl_3$ are plotted. In Figure 9a, the amide I IR spectrum of RA appears to be a doublet with two peaks at 1636 and 1676 cm^{-1}, which are close to the two peak frequencies of 1625 and 1671 cm^{-1} in that of PA. This indicates that RA and PA have a similar peptide backbone conformation, which is stabilized by the C_7-forming H-bonding interaction. Note that the backbone conformations are similar between RA and PA despite their inherently different preferences for the pyrrolidine ring conformations (C^γ-exo vs C^γ-endo).[26] For RE, the amide I vibration at the acetyl end exhibits a singlet at 1652 cm^{-1} and the C═O stretching vibration at the ester end exhibits a singlet at 1746 cm^{-1}. In Figure 9b, the azido IR spectrum of RA (RE) is a singlet at 2107 (2107) cm^{-1}, indicating that the local electrostatic environments around the azido groups in all the possible conformers are similar to one another and independent of the peptide backbone conformation in RA and RE. Furthermore, from the geometry-optimized structures of RA and RE, it is expected that the azido group free from any intramolecular electrostatic interactions with backbone peptides is fully solvated by chloroform. Note that the amide A IR spectrum of RA appears to be a doublet with two peaks at 3336 and 3450 cm^{-1}, which are close to two peak frequencies of 3327 and 3450 cm^{-1} in that of PA (see Figure S3 of the Supporting Information).

Ac-(4S)-Azp-(NH/O)Me. In Figure 9, the amide I and azido IR spectra of SA and SE in $CHCl_3$ are plotted. In Figure 9a, the amide I IR spectrum of SA appears to be a triplet with three peaks at 1635, 1652, and 1675 cm^{-1}. As will be shown later, however, it is more likely to be a quartet with an additional peak at 1664 cm^{-1}. For SE, the amide I vibration at the acetyl end exhibits a singlet at 1652 cm^{-1} and the C═O stretching vibration at the ester end exhibits a doublet with two peaks at 1734 and 1752 cm^{-1}. These results indicate that the local environments around the backbone peptides in SA (SE) are different from those in PA (PE) and RA (RE). Note that such local environments differ between SA (SE) and PA (PE) despite their inherently similar preferences for the pyrrolidine ring conformations (C^γ-endo).[26] In Figure 9b, the azido IR spectrum of SA (SE) is a doublet with two peaks at 2106 and 2127 (2107 and 2127) cm^{-1}. This indicates that there are two spectrally and conformationally different azido groups having different local electrostatic environments in SA and SE. Note that the amide A IR spectrum of SA appears to be a doublet with two peaks at 3332 and 3446 cm^{-1}, which are close to two peak frequencies of 3327 and 3450 (3336 and 3450) cm^{-1} in that of PA (RA) (see Figure S3 of the Supporting Information).

Recently, we studied the vibrational dynamics of nitrile stretch modes in a series of cyanophenols by using the IR pump−probe method.[56] Also, Cheatum and co-workers investigated the azido stretching vibration in 3-azidopyridine.[57] In these cases, a Fermi resonance peak appears close to the nitrile or azido stretch band. It was shown that the C−H bending modes in the aromatic ring participate in such Fermi resonance coupling. However, the high-frequency shoulder peak at 2127 cm^{-1} in the azido IR spectra of SA and SE is not related to such Fermi resonance peak. To verify this experimentally, we synthesized *N*-methyl (3*R*)- and (3*S*)-azidopyrrolidine compounds and examined their azido IR spectra in $CHCl_3$. It is found that the two spectra appear to be identical singlets at 2103 cm^{-1} without showing any notable shoulder peak at all (data not shown). We also examined the azido IR spectrum of the β-azidoalanine (Aza) derivative (Ac-Aza-NHMe) in $CHCl_3$.[40] It is found that its spectrum appears to be a singlet at 2111 cm^{-1} without exhibiting any shoulder peak. Furthermore, RA and RE show no such shoulder peak at all. Altogether, it seems that unlike aromatic 3-azidopyridine, these aliphatic azido derivatives do not show a shoulder peak in their azido IR spectra. Consequently, the shoulder peak in the azido IR spectra of SA and SE is not likely to be a Fermi resonance peak. As will be shown later, the shoulder peak arises from the asymmetric stretch of the bound azido group that makes a strong (weak) intramolecular electrostatic interaction with the C-terminal carbonyl O atom in SA (SE) (see Figure 7, upper left (lower)). On the other hand, the main peak arises from the asymmetric stretch of the free azido group that does not make such electrostatic interaction. Accordingly, the shoulder peak in the azido IR spectra of SA and SE originates from the bound azido conformation rather than Fermi resonance coupling.

Component Analyses of FTIR Spectra. From the NMR study and quantum chemistry calculations, we found that there are differences in the conformational propensities and intramolecular interactions between SA (SE) and RA (RE) and between SA (RA) and SE (RE). From the above IR study, it is found that the amide I and azido IR spectra are different depending on the azido configuration (SA (SE) vs RA (RE)) and C-terminal structure (SA (RA) vs SE (RE)). To elucidate the origin of such IR spectral differences, we examined the amide I and azido IR spectra of SA in detail and thereby the possible conformational distribution. As discussed in section III.A, such conformational distribution is suggested to be modulated by the azido configurations via stereoelectronic effects on the intramolecular interactions.

As shown in Figure 10a, the amide I IR spectrum of SA in $CHCl_3$ is composed of four bands and can be successfully fitted to four Gaussian functions at the center frequencies of 1635 (ν_1), 1652 (ν_1'), 1664 (ν_2'), and 1675 (ν_2) cm^{-1}. The three (ν_1, ν_1', and ν_2) of these four amide I bands directly correspond to those of PA in Figure 8, even though their relative areas differ between SA and PA. Note that in the case of SA (PA), the s-trans

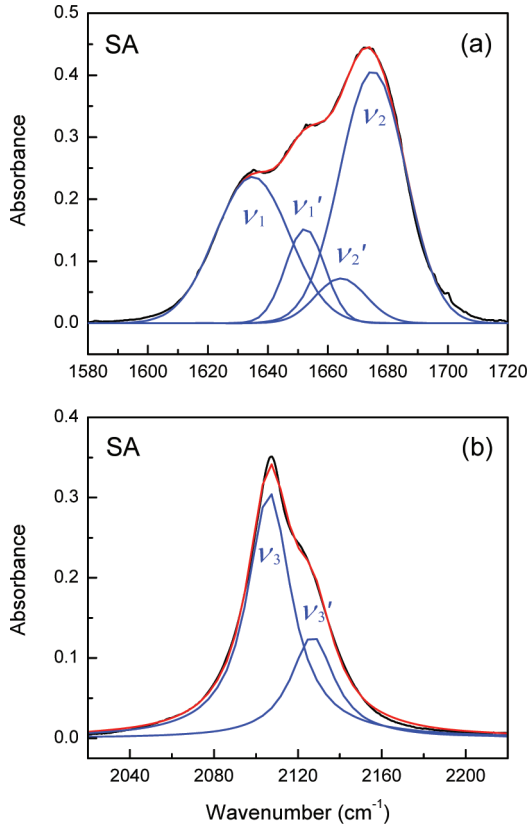

Figure 10. Factor analyses of the amide I and azido IR spectra of SA. In (a), the experimentally measured amide I IR spectrum (black) of SA, which is taken from Figure 9a, can be fitted to the sum (red) of four Gaussian functions (blue) at the center frequencies of 1635 (ν_1), 1652 (ν_1'), 1664 (ν_2'), and 1675 (ν_2) cm^{-1}. The two low (high)-frequency bands ν_1 and ν_1' (ν_2 and ν_2') can be assigned to the amide I modes localized on the acetyl (methylamide)-end peptide groups of the s-trans and s-cis conformers in SA, respectively.[25,53,54] In (b), the experimentally measured azido IR spectrum (black) of SA, which is taken from Figure 9b, can be fitted to the sum (red) of two Lorentzian functions (blue) at the center frequencies of 2106 (ν_3) and 2127 (ν_3') cm^{-1}. The low (high)-frequency ν_3 (ν_3')-band arises from the asymmetric stretch of the free (bound) azido group that does not make (makes) a strong intramolecular electrostatic interaction with the methylamide carbonyl O atom.[41] See the detailed discussion in section III.B. For quantitative fitting information, see Table S3 of the Supporting Information.

conformer is spectrally distinguishable (indistinguishable) from some (any) s-cis conformer in the amide I vibration at the methylamide end. The $n \rightarrow \pi^*$ interaction between the azido inner N^{δ} atom and the methylamide carbonyl C atom in the s-cis conformer of SA is responsible for the red-shift (~11 cm^{-1} from ν_2 to ν_2') of its amide I vibration at the methylamide end.[25] A similar red-shift was observed for SE, where the C═O stretching vibration at the ester end for the s-cis conformer is red-shifted by ~18 cm^{-1} (= 1752−1734 cm^{-1}) in comparison with that for the s-trans conformer (Figure S4a of the Supporting Information). The magnitude of the red-shift in such vibration for SE is similar to that for Ac-(4*S*)-Mop-OMe (~20 cm^{-1} = 1752−1732 cm^{-1}; see Figure S1 of the Supporting Information in ref 28). The relative areas of the four amide I bands (ν_1, ν_1', ν_2', and ν_2) in SA are found to be 4.78:1.63:1:7.32. The relative oscillator strengths of the three modes (ν_1, ν_1', and ν_2) were already determined to be 1.12:1:1.33 for PA in the above subsection. Assuming that the relative oscillator strengths of the two modes (ν_2' and ν_2) are the same, those of the four amide I modes (ν_1, ν_1', ν_2', and ν_2) in SA can be determined to be 1.12:1:1.33:1.33. Now, the relative populations of the four amide I oscillators in SA can be obtained by dividing the relative area of each band by the corresponding relative extinction coefficient. As a result, we found that the relative populations of the four amide I oscillators in SA are 5.7:2.2:1:7.3. Note that the relative area of the middle ν_1'-band in SA is larger compared to those in PA and RA, which show a triplet (ν_1, ν_1', and ν_2) and a doublet (ν_1 and ν_2), respectively (Table S3 of the Supporting Information). This IR result indicates the lower s-trans/s-cis ratio for SA compared to PA (RA) as found by NMR study (2.6 vs 6.9 (12.2), see Table 1). A similar lower s-trans/s-cis ratio for SE compared to PE (RE) is indicated in the C═O stretching vibration at the ester end. Unlike PE and RE, SE shows a doublet with two peaks at 1734 and 1752 cm^{-1} in that IR spectral region, where the low- and high-frequency bands can be easily assigned to the C═O stretching vibration at the ester ends of the s-cis and s-trans conformers in SE, respectively.[28] Note that the relative areas of the low- and high-frequency bands in SE are 1:1.94 (see Table S3 of the Supporting Information). This IR result indicates the lower s-trans/s-cis ratio for SE compared to PE (RE) as found by NMR study (1.9 vs 4.0 (3.9), see Table 1).

As shown in Figure 10b, the azido IR spectrum of SA in $CHCl_3$ is composed of two bands and can be successfully fitted to two Lorentzian functions at the center frequencies of 2106 (ν_3) and 2127 (ν_3') cm^{-1}. The same low-frequency ν_3-band appears in the azido IR spectra of RA, RE, and SE. This suggests that the low-frequency ν_3-band of SA arises from the asymmetric stretch of the free azido group that does not make any intramolecular electrostatic interactions with backbone peptides. On the other hand, the high-frequency ν_3'-band of SA arises from the asymmetric stretch of the bound azido group that makes a strong intramolecular electrostatic interaction with the methylamide carbonyl O atom in the s-trans conformer of SA (Figures 7, upper left). The high-frequency ν_3'-band of SA is blue-shifted by ~21 cm^{-1} from its low-frequency ν_3-band. The origin of such blue-shift can be elucidated by the vibrational solvatochromism theory recently developed to quantitatively describe the FTIR spectrum of azidomethane in solutions.[41] There, we showed that a blue-shift of the azido stretch mode can be induced by the electrostatic interaction between the azido central N atom and the negatively charged atom, such as the water and carbonyl O atom. This is because such electrostatic interaction increases the electron density of the azido group's π rather than π^* orbital, so that its π bonding is strengthened, its bond length is shortened, and thereby the azido stretch force constant increases. A similar blue-shift was observed for SE, where the high-frequency band is blue-shifted by ~20 cm^{-1} (= 2127−2107 cm^{-1}) from the low-frequency band (Figure S4b of the Supporting Information). The relative areas of the two azido stretch bands (ν_3 and ν_3') in SA are found to be 2.41:1. Assuming that the relative oscillator strengths of these two modes are the same, we found that the relative populations of the two azido stretch oscillators in SA are 2.4:1. For SE, those are 4.0:1.

Until now, we have emphasized the conformations of the *N*-acetyl group (s-trans and s-cis) and the pyrrolidine ring (C^{γ}-exo and C^{γ}-endo) only. However, it should also be noted that the azido group can undergo internal rotations. Consequently, there could be three azido conformers (*trans* or *anti* (*t*),

dx.doi.org/10.1021/jp1085119 |*J. Phys. Chem. B* 2012, 116, 5097–5110

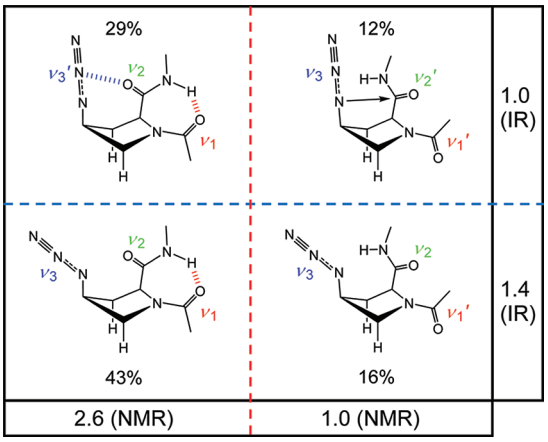

Figure 11. Four possible conformers of C^{γ}-endo-SA. Their relative populations were determined by ^{1}H NMR and FTIR spectroscopy. The s-trans (s-cis) conformers are shown on the left (right) side and the azido conformers having (no) intramolecular interactions between the azido group and the backbone peptide are shown in the upper (lower) part. In the upper left (right) conformer, which is the same as that in Figure 7, there is a strong intramolecular electrostatic ($n \rightarrow \pi^*$) interaction between the azido central N^{ε} (inner N^{δ}) atom and the methylamide carbonyl O (C) atom as indicated by a blue hashed line (black arrow). In the lower two conformers, however, there are no such electrostatic and $n \rightarrow \pi^*$ interactions. The C_7-forming H-bonding interaction is indicated by a red hashed line. The relative populations of the four conformers are obtained as described in section III.B.

gauche+ (g^+), and *gauche*− (g^-)), which are defined by the dihedral angle χ^5 ($C^{\delta}-C^{\gamma}-N^{\delta}-N^{\varepsilon}$) (see Figure 5). In the one SA conformer (see Figures 7 and 11, upper left (right)) having the C^{γ}-endo and s-trans (s-cis) conformations, the azido group can make a strong intramolecular electrostatic ($n \rightarrow \pi^*$) interaction with the methylamide carbonyl O (C) atom. In the other SA conformers (see Figure 11, lower), the azido group can make neither electrostatic nor $n \rightarrow \pi^*$ interaction. It may be suggested that the azido groups making (no) intramolecular interactions with the backbone peptide in SA are near *t* (g^+ plus g^-) and g^- (*t* plus g^+) to C^{δ} in the C^{γ}-endo structures of its s-trans and s-cis conformers, respectively. In a brief sense, we can therefore consider C^{γ}-endo-SA to exist apparently in the four possible conformations shown in Figure 11. These four conformers are spectrally different depending on the conformations of the *N*-acetyl (s-trans vs s-cis) and azido (bound vs free) groups. First, the two s-trans conformers (see Figure 11, left) are spectrally different from the two s-cis conformers (see Figure 11, right) in the amide I vibration at the acetyl end (ν_1 vs ν_1'). The C_7-forming H-bonding interaction between the *N*-acetyl carbonyl O atom and the methylamide H atom in the s-trans conformer of SA is responsible for the red-shift (from ν_1' to ν_1) of its amide I vibration at the acetyl end.[54] Second, the one conformer (see Figure 11, upper right) is spectrally distinguishable from the other three conformers in the amide I vibration at the methylamide end so that they are treated as separate spectroscopic species (ν_2' vs ν_2). Note that the one s-cis conformer (see Figure 11, lower right) is assumed to be spectrally indistinguishable from the two s-trans conformers (see Figure 11, left) in the amide I vibration at the methylamide end (see Figure 8). The $n \rightarrow \pi^*$ interaction between the azido inner N^{δ} atom and the methylamide carbonyl C atom in the s-cis conformer of SA is responsible for the red-shift (from ν_2 to ν_2') of its amide I vibration at the methylamide end.[25] Third, the one conformer (see Figure 11, upper left) is spectrally different from the other three conformers in the azido stretch mode (ν_3' vs ν_3). The strong electrostatic interaction between the azido central N^{ε} atom and the methylamide carbonyl O atom in the s-trans conformer of SA is responsible for the blue-shift (from ν_3 to ν_3') of its azido stretch mode.[41] Consequently, a mixture of the four SA conformers shown in Figure 11 is expected to exhibit the four amide I bands (ν_1, ν_1', ν_2', and ν_2) and the two azido stretch bands (ν_3 and ν_3') shown in Figure 10.

Now, we can estimate the relative populations of the four SA conformers from the NMR and FTIR analyses. From the NMR study, the s-trans/s-cis ratio for SA in $CHCl_3$ was found to be 2.6:1. Thus, the population ratio of the left to right two conformers in Figure 11 is 2.6:1. From the above IR study, the relative populations of the two azido stretch oscillators (ν_3 and ν_3') in SA are found to be 2.4:1. Thus, the population ratio of the one conformer (see Figure 11, upper left) to the other three conformers is 1:2.4. In addition, from the above IR study, the relative populations of the two amide I oscillators at the methylamide end (ν_2 and ν_2') in SA are found to be 7.3:1. Thus, the population ratio of the one conformer (see Figure 11, upper right) to the other three conformers is 1:7.3. By combining these three results, we found the percent populations of the four SA conformers, as shown in Figure 11. These results can be used to calculate the relative populations of the four amide I oscillators (ν_1, ν_1', ν_2', and ν_2) in SA, which are 6.0:2.3:1:7.3. Note that this calculated ratio is in good agreement with the experimentally measured ratio of 5.7:2.2:1:7.3 for SA presented above.

C. Frequency-Resolved IR Pump−Probe Spectroscopy. In the previous subsections, the amide I and azido IR spectra were analyzed to extract information about the relative populations of the four SA conformers shown in Figure 11. It is found that there are two types of azido groups having different local electrostatic environments in SA, as evidenced by the two azido stretch bands (ν_3 and ν_3') in Figure 10b. Their local electrostatic environments are dependent on intramolecular interactions, which are different depending on the conformations of the *N*-acetyl (s-trans vs s-cis) and azido (bound vs free) groups. In the one SA conformer (see Figures 7 and 11, upper left) having the C^{γ}-endo and s-trans conformations, the azido group can make a strong intramolecular electrostatic interaction with the methylamide carbonyl O atom. Such electrostatic interaction increases the electron density of the azido group's π orbital, thereby increasing the azido stretch force constant. In the other three SA conformers (see Figures 7 and 11), however, the azido group cannot make such electrostatic interaction. As a result, the azido stretch band (ν_3') of one such conformer is blue-shifted from those (ν_3) of the other three conformers (see Figure 10b). A similar blue-shift also occurs in SE, even though the relative populations of the two azido stretch oscillators (ν_3 and ν_3') in SE become higher compared to those in SA (4.0:1 vs 2.4:1, see Figure 10b and Figure S4b of the Supporting Information). To further study the local electrostatic environments of the azido group in detail, we carried out time- and frequency-resolved IR pump−probe experiments. The vibrational population relaxation dynamics thus obtained has been found to be very sensitive to the local electrostatic environments of the vibrational probes such as the azido group.[58−60]

A typical frequency-resolved (dispersed) pump−probe signal for a single anharmonic oscillator shows both positive and negative peaks with high- and low-frequencies, respectively. Let $|0\rangle$, $|1\rangle$, and $|2\rangle$ denote the vibrational ground, first excited,

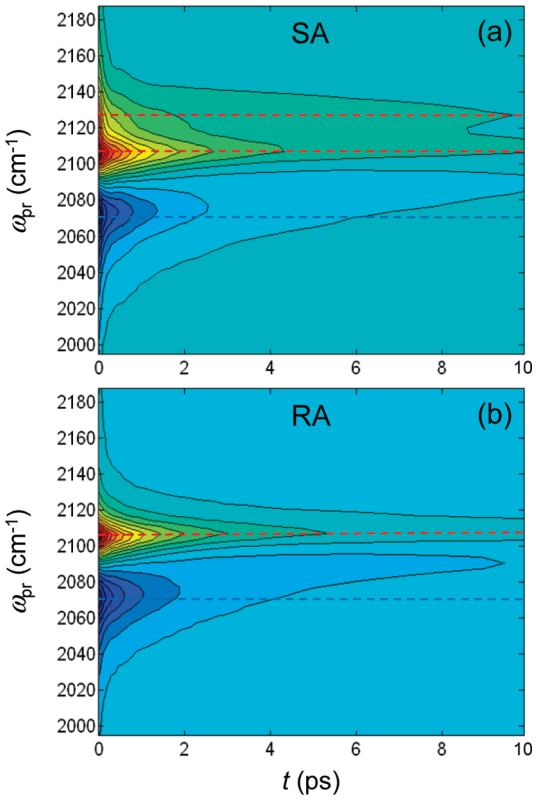

Figure 12. Time- and frequency-resolved femtosecond IR pump−probe signals for the azido stretch modes of SA (a) and RA (b). See experimental details in sections II.B and II.E. The dashed lines highlight the probe frequencies with positive (red) and negative (blue) signals. The population decay rates can be estimated from the time profile of the IR pump−probe signal at these particular probe frequencies, as shown in Figure 13. The population decay rate at 2127 cm^{-1} corresponds to the excited-state lifetime of the azido stretch mode in the one SA conformer, where the azido group makes a strong intramolecular electrostatic interaction with the methylamide carbonyl O atom (see Figures 7 and 11, upper left). On the other hand, the population decay rates at 2107 and 2070 cm^{-1} correspond to the excited-state lifetimes of the azido stretch modes in the SA and RA conformers, where the azido group does not make such electrostatic interaction (see Figures 6, 7, and 11). See the detailed discussion in section III.C.

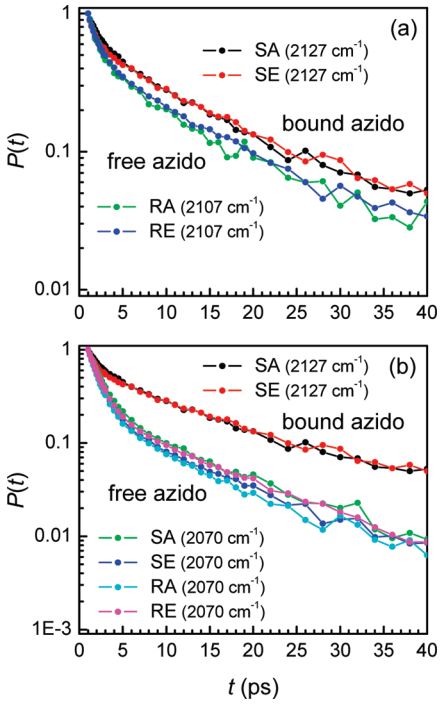

Figure 13. Population relaxation decays, $P(t)$, of the azido stretch modes in SA, SE, RA, and RE at different probe frequencies. In (a), $P(t)$'s of the azido stretch modes in SA and SE at 2127 cm^{-1} ($v = 0 \rightarrow 1$ transition) and in RA and RE at 2107 cm^{-1} ($v = 0 \rightarrow 1$ transition) are plotted. In (b), those in SA and SE at 2127 cm^{-1} ($v = 0 \rightarrow 1$ transition) and in SA, SE, RA, and RE at 2070 cm^{-1} ($v = 1 \rightarrow 2$ transition) are plotted. See experimental details in sections II.B and II.E. These plots are obtained from the IR pump−probe signals in Figure 12 and Figure S5 of the Supporting Information. Note that $P(t)$'s in SA and SE at 2127 cm^{-1} (in RA and RE at 2107 cm^{-1} and in SA, SE, RA, and RE at 2070 cm^{-1}) provide information about the exited-state lifetime of the bound (free) azido group. See the detailed discussion in section III.C. For quantitative fitting information, see Table 2.

and second excited (overtone) states, respectively. Then, the high-frequency positive peak is associated with the ground-state bleach ($v = 0 \rightarrow 1$ transition) and the stimulated emission ($v = 1 \rightarrow 0$ transition), whereas the low-frequency negative peak is associated with the excited-state absorption ($v = 1 \rightarrow 2$ transition). The frequency difference between the positive and negative peaks is related to the vibrational anharmonicity as well as the line broadening. As shown in ref 56, the frequency-resolved pump−probe signal can be approximately written as a sum of positive and negative Gaussian functions. Here, the center frequencies of these two Gaussian functions correspond to the $0 \rightarrow 1$ and $1 \rightarrow 2$ transition frequencies, denoted ω_{10} and $\omega_{21} = \omega_{10} - \Delta\omega$, where $\Delta\omega$ is the vibrational anharmonic frequency shift. Thus, the dispersed pump−probe spectrum at a given delay time t can be written as

$$S(\omega) = A_{HF} \exp\left(\frac{-(\omega - \omega_{10})^2}{2\Omega_{10}^2}\right) - A_{LF} \exp\left(\frac{-(\omega - \omega_{21})^2}{2\Omega_{21}^2}\right) \quad (1)$$

where A_{HF} and A_{LF} represent the time-dependent amplitudes of the $0 \rightarrow 1$ and $1 \rightarrow 2$ transitions, respectively. The corresponding Gaussian widths denoted Ω_{10} and Ω_{21} represent the vibrational bandwidths associated with the $0 \rightarrow 1$ and $1 \rightarrow 2$ transitions. Here, for simplicity, the spectral diffusion causing the time-dependent shifts of the center frequencies at a very short time is ignored.

Table 2. Population Relaxation Decays of Azido Stretch Modes at Different Probe Frequencies[a]

	probe frequency (cm^{-1})	a_1	τ_1 (ps)	a_2	τ_2 (ps)
RA ($v = 1 \rightarrow 2$)	2070	1.78	1.24	0.22	9.63
RA ($v = 0 \rightarrow 1$)	2107	1.32	1.23	0.44	12.57
RE ($v = 1 \rightarrow 2$)	2070	1.64	1.37	0.23	11.34
RE ($v = 0 \rightarrow 1$)	2107	1.22	1.27	0.47	13.12
SA ($v = 1 \rightarrow 2$)	2070	1.50	1.48	0.25	10.97
SA ($v = 0 \rightarrow 1$)	2127	0.84	1.60	0.57	14.14
SE ($v = 1 \rightarrow 2$)	2070	1.66	1.37	0.21	10.71
SE ($v = 0 \rightarrow 1$)	2127	1.20	1.00	0.58	14.36

[a] Biexponential fit to the IR pump−probe signal from 1.0 to 70 ps (see Figure 13). The IR pump−probe signals are normalized at $t = 1.0$ ps. See experimental details in sections II.B. and II.E and the detailed discussion in section III.C.

dx.doi.org/10.1021/jp1085119 |J. Phys. Chem. B 2012, 116, 5097–5110

Figure 12 displays the frequency-resolved IR pump−probe signals for the azido stretch modes of SA and RA. In the case of SA, there are two different azido stretch oscillators so that the transient IR pump−probe spectrum should consist of two positive and two negative peaks. As shown in Figure 12a, however, one cannot fully frequency-resolve these four peaks. This is due to the significant spectral overlaps, much like the spectrally congested azido IR spectrum in Figure 10b. Nevertheless, one can still identify two positive peaks at 2127 and 2107 cm^{-1} (see the red dashed lines in Figure 12a) and one negative peak at 2070 cm^{-1}(blue dashed line). Furthermore, it is interesting to note that the excited state of the high-frequency component at 2127 cm^{-1} appears to have a longer lifetime. Here, it should be mentioned again that the high-frequency azido stretch mode at 2127 cm^{-1} is associated with the one SA conformer, where the azido group makes a strong intramolecular electrostatic interaction with the methylamide carbonyl O atom (see Figures 7 and 11, upper left). In the case of RA, the IR pump−probe signal exhibits a typical pattern of one positive and one negative peak decaying monotonically in time at 2107 and 2070 cm^{-1}, respectively (see the red and blue dashed lines in Figure 12b). Note that the azido stretch modes at 2107 and 2070 cm^{-1} are associated with the RA and SA conformers, where the azido group does not make such electrostatic interaction (see Figures 6, 7, and 11). For comparison, we also measured the frequency-resolved IR pump−probe signals for SE and RE (Figure S5 of the Supporting Information).

Figure 13a displays the population relaxation decays of the azido stretch modes in SA and SE at 2127 cm^{-1} ($v = 0 \rightarrow 1$ transition) and in RA and RE at 2107 cm^{-1} ($v = 0 \rightarrow 1$ transition). The population relaxation decays are found to be biexponential, and the fitting results are summarized in Table 2. It is observed that the population relaxation dynamics of the azido stretch mode at 2127 cm^{-1} in SA is quantitatively similar to that in SE. This indicates that the local electrostatic environments of the bound azido groups in SA and SE are very similar. We found that the exicted states ($v = 1$) of the azido stretch modes in SA and SE at 2127 cm^{-1} have longer lifetimes in comparison to those in RA and RE at 2107 cm^{-1}. This indicates that the excited-state lifetimes of the bound azido groups in SA and SE are longer than those of the free azido groups in RA and RE.

Figure 13b displays the population relaxation decays of the azido stretch modes in SA and SE at 2127 cm^{-1} ($v = 0 \rightarrow 1$ transition) and in SA, SE, RA, and RE at 2070 cm^{-1} ($v = 1 \rightarrow 2$ transition). Again, the decaying patterns of SA, SE, RA, and RE at 2070 cm^{-1} are biexponential (see Table 2). It is observed that the population relaxation dynamics of the azido stretch mode at 2070 cm^{-1} in SA is quantitatively similar to those in SE, RA, and RE. This indicates that the local electrostatic environments of the free azido groups in SA, SE, RA, and RE are quite similar. We found that the exicted states ($v = 1$) of the azido stretch modes in SA and SE at 2127 cm^{-1} have longer lifetimes in comparison to those in SA, SE, RA, and RE at 2070 cm^{-1}. Furthermore, it is shown that the population decay rates for the $v = 0 \rightarrow 1$ and $v = 1 \rightarrow 2$ transitions are different in SA and SE, but similar in RA and RE. In general, the population decay rate for the $v = 0 \rightarrow 1$ transition is not necessarily the same as that for the $v = 1 \rightarrow 2$ transition, if there are intermediate states. These indicate that there are two conformationally different azido groups (bound and free) in SA and SE, whereas there is only a free azido group in RA and RE. In addition, the excited-state lifetimes of the bound azido groups in SA and SE are longer than those of the free azido groups in SA, SE, RA, and RE. As described above, the bound azido group exhibits the shoulder peak at 2127 cm^{-1}, whereas the free azido group exhibits the main peak at 2107 cm^{-1}. That is, the shoulder peak originates from the bound azido conformation rather than Fermi resonance coupling, as discussed in section III.B. This is further indicated in the early time profile of the IR pump−probe signal for the azido stretch modes of SA (Figure S6 of the Supporting Information) and in the azido 2DIR spectrum of SA at early waiting times (data not shown). They provide evidence that the shoulder peak is not likely to be a Fermi resonance peak.

Generally, it is expected that the population relaxation decay of the strongly interacting azido stretch mode is likely to be faster than that of the comparatively free one. This can be a reasonable picture only when such intramolecular interactions act like the main channel for its intramolecular vibrational relaxation (IVR). In the present case, however, it was found that the excited states ($v = 1$) of the free azido stretch modes in SA, SE, RA, and RE have a bit shorter lifetimes. Here, the ultrafast (<5 ps) component in $P(t)$ cannot be the vibrational relaxation of the azido stretch mode directly to the solvent bath ($CHCl_3$). Thus, we need to consider two possible IVR pathways through anharmonic couplings with delocalized modes in either the pyrrolidine ring or the backbone peptides via electrostatic or $n \rightarrow \pi^*$ interaction. To examine the latter possibility, let us consider the molecular structures of the upper two conformers of SA in Figures 7 and 11. There, the intramolecular electrostatic or $n \rightarrow \pi^*$ interaction is in the direction nearly orthogonal to the transition dipole of the azido stretch mode. Thus, it is believed that the IVR from the intramolecularly interacting azido group to the C-terminal peptide vibrations is less effective than that from the free azido group to low-frequency modes in the pyrrolidine ring. A quantitative explanation of these IVR processes requires complete information about the multidimensional potential energy surface with accurate anharmonic couplings. However, this is beyond the scope of this work. It would be very interesting to study such molecular structure-dependent IVR rates by carrying out quantum mechanical/molecular mechanical molecular dynamics simulations in the future.

IV. SUMMARY

In the present paper, we studied the conformations of four 4-azidoproline (Azp) derivatives, RA, RE, SA, and SE, by using spectroscopic methods in combination with quantum chemistry calculations. From the ^1H NMR study, it is found that their s-trans/s-cis ratio is different depending on the azido configuration (4*R* vs 4*S*) and C-terminal structure (methylamide vs ester). In addition, both the s-trans and s-cis conformers in the 4*R* (4*S*) configuration are found to adopt the C^γ-exo (C^γ-endo) conformation, where the azido group on the pyrrolidine ring occupies the pseudoaxial position. The origin of the differences in such conformational propensities between 4*R* and 4*S* configurations and between C-terminal methylamide and ester ends was elucidated by quantum chemistry calculations with DFT-IEFPCM. It is found that the azido configurations and C-terminal structures affect intramolecular interactions, which are responsible for the ensuing conformational adoption by Azp. Importantly, the Azp conformations modulated by the azido configurations are found to be probed by IR spectroscopy. From the combined NMR and IR results, the relative populations of the four SA conformers that differ in the conformations of the

N-acetyl and azido groups were determined. There, it is found that there are two types of azido groups having different local electrostatic environments in SA, which were further investigated by time- and frequency-resolved IR pump−probe spectroscopy. Taken together, 4-azidoproline can be both a structure-control and -probing element, which enables the infrared tracking of proline roles in the structure, function, and dynamics of proteins including ion channel, amyloid precursor protein, and intrinsically disordered protein.

■ ASSOCIATED CONTENT

Supporting Information. Complete author list for ref 49, detailed synthetic procedures and characterization for compounds, and figures and tables exhibiting the results of IR and NMR spectroscopic studies. This material is available free of charge via the Internet at http://pubs.acs.org.

■ AUTHOR INFORMATION

Corresponding Author

*E-mail: mcho@korea.ac.kr (M.C.); hogyuhan@korea.ac.kr (H.H.).

■ ACKNOWLEDGMENT

This work was supported by the NRF (No. 2009-0078897) and KBSI (T31401) grants to M.C. and the NRF (No. 2010-0022070) and KBSI (T31401) grants to H.H.

■ REFERENCES

(1) Yaron, A.; Naider, F. *Crit. Rev. Biochem. Mol. Biol.* **1993**, *28*, 31–81.
(2) Williamson, M. P. *Biochem. J.* **1994**, *297*, 249–260.
(3) Vanhoof, G.; Goossens, F.; De Meester, I.; Hendriks, D.; ScharpÉ, S. *FASEB J.* **1995**, *9*, 736–744.
(4) MacArthur, M. W.; Thornton, J. M. *J. Mol. Biol.* **1991**, *218*, 397–412.
(5) Reimer, U.; Scherer, G.; Drewello, M.; Kruber, S.; Schutkowski, M.; Fischer, G. *J. Mol. Biol.* **1998**, *279*, 449–460.
(6) Jenkins, C. L.; Raines, R. T. *Nat. Prod. Rep.* **2002**, *19*, 49–59.
(7) Brodsky, B.; Persikov, A. V. *Adv. Protein Chem.* **2005**, *70*, 301–339.
(8) Bryan, M. A.; Brauner, J. W.; Anderle, G.; Flach, C. R.; Brodsky, B.; Mendelsohn, R. *J. Am. Chem. Soc.* **2007**, *129*, 7877–7884.
(9) Lee, W. Y.; Sine, S. M. *Nature* **2005**, *438*, 243–247.
(10) Lummis, S. C. R.; Beene, D. L.; Lee, L. W.; Lester, H. A.; Broadhurst, R. W.; Dougherty, D. A. *Nature* **2005**, *438*, 248–252.
(11) Pastorino, L.; Sun, A.; Lu, P.-J.; Zhou, X. Z.; Balastik, M.; Finn, G.; Wulf, G.; Lim, J.; Li, S.-H.; Li, X.; Xia, W.; Nicholson, L. K.; Lu, K. P. *Nature* **2006**, *440*, 528–534.
(12) Fischer, G. *Chem. Soc. Rev.* **2000**, *29*, 119–127.
(13) Dugave, C.; Demange, L. *Chem. Rev.* **2003**, *103*, 2475–2532.
(14) Shoulders, M. D.; Raines, R. T. *Annu. Rev. Biochem.* **2009**, *78*, 929–958.
(15) Hinderaker, M. P.; Raines, R. T. *Protein Sci.* **2003**, *12*, 1188–1194.
(16) Bartlett, G. J.; Choudhary, A.; Raines, R. T.; Woolfson, D. N. *Nat. Chem. Biol.* **2010**, *6*, 615–620.
(17) Madison, V.; Schellman, J. *Biopolymers* **1970**, *9*, 511–567.
(18) DeTar, D. F.; Luthra, N. P. *J. Am. Chem. Soc.* **1977**, *99*, 1232–1244.
(19) Madison, V.; Kopple, K. D. *J. Am. Chem. Soc.* **1980**, *102*, 4855–4863.
(20) Liang, G.-B.; Rito, C. J.; Gellman, S. H. *Biopolymers* **1992**, *32*, 293–301.
(21) Kang, Y. K. *J. Phys. Chem. B* **2006**, *110*, 21338–21348.
(22) Gao, J.; Kelly, J. W. *Protein Sci.* **2008**, *17*, 1096–1101.
(23) Taylor, C. M.; Hardré, R.; Edwards, P. J. B.; Park, J. H. *Org. Lett.* **2003**, *5*, 4413–4416.
(24) Holmgren, S. K.; Taylor, K. M.; Bretscher, L. E.; Raines, R. T. *Nature* **1998**, *392*, 666–667.
(25) Bretscher, L. E.; Jenkins, C. L.; Taylor, K. M.; DeRider, M. L.; Raines, R. T. *J. Am. Chem. Soc.* **2001**, *123*, 777–778.
(26) DeRider, M. L.; Wilkens, S. J.; Waddell, M. J.; Bretscher, L. E.; Weinhold, F.; Raines, R. T.; Markley, J. L. *J. Am. Chem. Soc.* **2002**, *124*, 2497–2505.
(27) Shoulders, M. D.; Satyshur, K. A.; Forest, K. T.; Raines, R. T. *Proc. Natl. Acad. Sci. U.S.A.* **2010**, *107*, 559–564.
(28) Shoulders, M. D.; Kotch, F. W.; Choudhary, A.; Guzei, I. A.; Raines, R. T. *J. Am. Chem. Soc.* **2010**, *132*, 10857–10865.
(29) Renner, C.; Alefelder, S.; Bae, J. H.; Budisa, N.; Huber, R.; Moroder, L. *Angew. Chem., Int. Ed.* **2001**, *40*, 923–925.
(30) Cadamuro, S. A.; Reichold, R.; Kusebauch, U.; Musiol, H.-J.; Renner, C.; Tavan, P.; Moroder, L. *Angew. Chem., Int. Ed.* **2008**, *47*, 2143–2146.
(31) Thomas, K. M.; Naduthambi, D.; Tririya, G.; Zondlo, N. J. *Org. Lett.* **2005**, *7*, 2397–2400.
(32) Thomas, K. M.; Naduthambi, D.; Zondlo, N. J. *J. Am. Chem. Soc.* **2006**, *128*, 2216–2217.
(33) Sonntag, L.-S.; Schweizer, S.; Ochsenfeld, C.; Wennemers, H. *J. Am. Chem. Soc.* **2006**, *128*, 14697–14703.
(34) Kümin, M.; Sonntag, L.-S.; Wennemers, H. *J. Am. Chem. Soc.* **2007**, *129*, 466–467.
(35) Erdmann, R. S.; Wennemers, H. *J. Am. Chem. Soc.* **2010**, *132*, 13957–13959.
(36) Owens, N. W.; Braun, C.; O'Neil, J. D.; Marat, K.; Schweizer, F. *J. Am. Chem. Soc.* **2007**, *129*, 11670–11671.
(37) Owens, N. W.; Stetefeld, J.; Lattová, E.; Schweizer, F. *J. Am. Chem. Soc.* **2010**, *132*, 5036–5042.
(38) Gorske, B. C.; Bastian, B. L.; Geske, G. D.; Blackwell, H. E. *J. Am. Chem. Soc.* **2007**, *129*, 8928–8929.
(39) Gorske, B. C.; Stringer, J. R.; Bastian, B. L.; Fowler, S. A.; Blackwell, H. E. *J. Am. Chem. Soc.* **2009**, *131*, 16555–16567.
(40) Oh, K.-I.; Lee, J.-H.; Joo, C.; Han, H.; Cho, M. *J. Phys. Chem. B* **2008**, *112*, 10352–10357.
(41) Choi, J.-H.; Oh, K.-I.; Cho, M. *J. Chem. Phys.* **2008**, *129*, 174512.
(42) Oh, K.-I.; Kim, W.; Joo, C.; Yoo, D.-G.; Han, H.; Hwang, G.-S.; Cho, M. *J. Phys. Chem. B* **2010**, *114*, 13021–13029.
(43) Ye, S.; Zaitseva, E.; Caltabiano, G.; Schertler, G. F. X.; Sakmar, T. P.; Deupi, X.; Vogel, R. *Nature* **2010**, *464*, 1386–1389.
(44) Taskent-Sezgin, H.; Chung, J.; Banerjee, P. S.; Nagarajan, S.; Dyer, R. B.; Carrico, I.; Raleigh, D. P. *Angew. Chem., Int. Ed.* **2010**, *49*, 7473–7475.
(45) Park, S.; Kwak, K.; Fayer, M. D. *Laser Phys. Lett.* **2007**, *4*, 704–718.
(46) Park, S.; Fayer, M. D. *Proc. Natl. Acad. Sci. U.S.A.* **2007**, *104*, 16731–16738.
(47) Park, K.-H.; Choi, S. R.; Choi, J.-H.; Park, S.; Cho, M. *ChemPhysChem* **2010**, *11*, 3632–3637.
(48) Lee, K.-K.; Park, K.-H.; Kwon, D.; Choi, J.-H.; Son, H.; Park, S.; Cho, M. *J. Chem. Phys.* **2011**, *134*, 064506.
(49) Frisch, M. J.; et al. *Gaussian 03*, revision E.01; Gaussian, Inc.: Wallingford, CT, 2004.
(50) Cancès, E.; Mennucci, B.; Tomasi, J. *J. Chem. Phys.* **1997**, *107*, 3032–3041.
(51) Tomasi, J.; Mennucci, B.; Cammi, R. *Chem. Rev.* **2005**, *105*, 2999–3093.
(52) Hahn, S.; Lee, H.; Cho, M. *J. Chem. Phys.* **2004**, *121*, 1849–1865.
(53) Lee, K.-K.; Hahn, S.; Oh, K.-I.; Choi, J. S.; Joo, C.; Lee, H.; Han, H.; Cho, M. *J. Phys. Chem. B* **2006**, *110*, 18834–18843.
(54) Oh, K.-I.; Han, J.; Lee, K.-K.; Hahn, S.; Han, H.; Cho, M. *J. Phys. Chem. A* **2006**, *110*, 13355–13365.
(55) Steffel, L. R.; Cashman, T. J.; Reutershan, M. H.; Linton, B. R. *J. Am. Chem. Soc.* **2007**, *129*, 12956–12957.

(56) Lee, K.-K.; Park, K.-H.; Choi, J.-H.; Ha, J.-H.; Jeon, S.-J.; Cho, M. *J. Phys. Chem. A* **2010**, *114*, 2757–2767.
(57) Nydegger, M. W.; Dutta, S.; Cheatum, C. M. *J. Chem. Phys.* **2010**, *133*, 134506.
(58) Bandaria, J. N.; Dutta, S.; Hill, S. E.; Kohen, A.; Cheatum, C. M. *J. Am. Chem. Soc.* **2008**, *130*, 22–23.
(59) Barbour, L. W.; Hegadorn, M.; Asbury, J. B. *J. Am. Chem. Soc.* **2007**, *129*, 15884–15894.
(60) Krummel, A. T.; Mukherjee, P.; Zanni, M. T. *J. Phys. Chem. B* **2003**, *107*, 9165–9169.
(61) IUPAC-IUB Commission on Biochemical Nomenclature *J. Mol. Biol.* **1970**, *52*, 1–17.

NOTE ADDED AFTER ASAP PUBLICATION

This paper was published on the Web on April 18, 2012. Figures 10 and 11 have been revised. The correct version was reposted on April 23, 2012.